STATISTICS, OPTIMIZATION AND INFORMATION COMPUTING
Stat., Optim. Inf. Comput., Vol. **17**, Month 2027, pp 0–22.
Published online in International Academic Press (www.IAPress.org)

A Voltage-Ratio Fixed-Point Formulation for Power Flow Analysis in Single-Phase AC Distribution Networks with Certified Convergence

Oscar Danilo Montoya [1*], Carlos Alberto Ramírez-Vanegas [2], and Fernando Mesa [2]

[1] *Facultad de Ingeniería, Universidad Distrital Francisco José de Caldas, Bogotá D.C. 110121, Colombia*
[2] *Departamento de Matemáticas, Facultad de Ciencias Básicas, Universidad Tecnológica de Pereira, Pereira 660003, Colombia*

Abstract This paper proposes a voltage-ratio fixed-point formulation for power-flow analysis in balanced AC distribution networks with radial or meshed topologies. The classical nodal power-flow equations are recast exactly in terms of inverse squared-voltage magnitude variables and pairwise complex voltage-ratio variables, and then compactly normalized with respect to the unique slack-bus voltage. The resulting normalized power-flow equations define a natural fixed-point mapping whose nonlinearity is confined to an element-wise reciprocal of the conjugated normalized voltage vector, thereby avoiding the explicit construction of the inverse of the reduced nodal admittance matrix. A convergence analysis is developed using the Banach fixed-point theorem. Sufficient conditions for the existence and uniqueness of the power-flow solution, as well as for the at-least-linear convergence of the proposed iteration, are derived explicitly in terms of the reduced nodal admittance matrix, the normalized complex power injections, the no-load voltage profile, and a certified contraction radius. The analysis is topology-agnostic in the sense that it does not rely on radiality assumptions, parent–child relationships, or backward/forward sweep orderings; it therefore applies, at the theoretical level, to radial and meshed networks with a unique slack bus, provided that the reduced nodal admittance matrix is nonsingular. The derived contraction factor also yields a priori and a posteriori error bounds, and a simplified sufficient condition is presented for practical verification. The numerical validation, however, is restricted to radial feeders: the formulation and its convergence certificate are tested on the IEEE 33-bus and IEEE 69-bus radial distribution test feeders, where the method converges to the same power-flow solution for all tested initial voltage magnitudes, with machine-precision agreement and iteration counts between 11 and 15. The computed voltage profiles agree with the classical benchmark results, and the computed power losses are consistent with them once the demand aggregation convention is taken into account; this provides evidence of the correctness of the formulation for radial networks. Meshed-network validation is identified as future work. The proposed approach offers a topology-agnostic formulation and convergence analysis for power-flow studies, which is particularly relevant for modern distribution systems with high penetration of distributed energy resources.

Keywords Power flow; Fixed-point iteration; Banach fixed-point theorem; Voltage-ratio formulation; Radial and meshed networks; Convergence analysis; Distribution systems

AMS 2010 subject classifications 46N10, 65H10, 90C30

DOI: 10.19139/soic-2310-5070-4665

Nomenclature

AC Alternating Current

*Correspondence to: O. D. Montoya (Email: odmontoyag@udistrital.edu.co). Facultad de Ingeniería, Universidad Distrital Francisco José de Caldas, Bogotá D.C. 110121, Colombia.

ISSN 2310-5070 (online) ISSN 2311-004X (print)
Copyright © 2027 International Academic Press

BFS	Backward/Forward Sweep
DER	Distributed Energy Resource
HELM	Holomorphic Embedding Load-Flow Method
NR	Newton–Raphson
PF	Power Flow

$\alpha(\rho)$	Contraction factor of the fixed-point mapping $\mathcal{F}$ over $\mathcal{D}_\rho$
$\mathbf{r}(\rho)$	Vector of normalized voltage-magnitude lower bounds $r_k(\rho)$
$\mathcal{D}_\rho$	Closed contraction domain centered at the no-load voltage profile $\mathbf{q}^0$
$\mathcal{F}(\mathbf{q})$	Fixed-point mapping in the normalized voltage coordinates
ρ	Radius of the contraction domain $\mathcal{D}_\rho$

Objective Function

$(\cdot)^*$	Complex conjugate
$(\cdot)^{-1}$	Matrix inverse
$(\cdot)^{\circ 2}$	Element-wise square
$(\cdot)^{\circ(-1)}$	Element-wise reciprocal
$(\cdot)^\mathsf{T}$	Transpose operator
$\mathrm{diag}(\cdot)$	Diagonal matrix operator
$\oslash$	Element-wise division
j	Imaginary unit, $j^2 = -1$

Parameters

$\boldsymbol{\sigma}$	Vector of normalized complex power injections at the non-slack buses
$\mathbf{D}_{\boldsymbol{\sigma}^*}$	Diagonal matrix of conjugated normalized complex power injections, $\mathbf{D}_{\boldsymbol{\sigma}^*} = \mathrm{diag}(\boldsymbol{\sigma}^*)$
$\mathbf{Y}$	Nodal admittance matrix [p.u.]
$\mathbf{y}_{0L}$	Admittance vector coupling the slack bus to the non-slack buses [p.u.]
$\mathbf{y}_{L0}$	Admittance vector coupling the non-slack buses to the slack bus [p.u.]
$\mathbf{Y}_{LL}$	Reduced nodal admittance matrix associated with the non-slack buses [p.u.]
ε	Convergence tolerance
n	Number of non-slack buses
P_k	Specified net active power injection at bus k [p.u.]
Q_k	Specified net reactive power injection at bus k [p.u.]

S_k Specified net complex power injection at bus k, $S_k = P_k + jQ_k$ [p.u.]

Y_{00} Slack-bus diagonal entry of the nodal admittance matrix [p.u.]

Y_{km} Entry (k, m) of the nodal admittance matrix [p.u.]

Sets

$\mathcal{L}$ Set of non-slack buses, $\mathcal{L} = \mathcal{N} \setminus \{0\}$

$\mathcal{N}$ Set of network buses, $\mathcal{N} = \{0, 1, \ldots, n\}$

k, m Bus indices, $k, m \in \mathcal{N}$

t Fixed-point iteration index

Variables

$\mathbf{q}$ Vector of slack-normalized complex voltages at the non-slack buses

$\mathbf{q}^{(t)}$ Normalized complex voltage vector at fixed-point iteration t

$\mathbf{q}^0$ Normalized no-load voltage profile, $\mathbf{q}^0 = -\mathbf{Y}_{LL}^{-1}\mathbf{y}_{L0}$

$\mathbf{q}^\star$ Fixed-point solution of the normalized power-flow equations within the certified contraction region

$\mathbf{V}_L$ Vector of complex voltages at the non-slack buses [p.u.]

q_k Slack-normalized complex voltage at bus k, $q_k = V_k/V_0$, with $q_k \neq 0$

R_{km} Complex voltage ratio between buses m and k, $R_{km} = V_m/V_k$

V_k Complex voltage at bus k [p.u.], $V_k \neq 0$

1. Introduction

1.1. Motivation

Power-flow analysis is the cornerstone of steady-state analysis, operation, planning, and control of electric power systems. In modern distribution networks, the growing penetration of distributed energy resources (DERs), such as photovoltaic generation, battery energy storage systems, and electric vehicles, has substantially increased the complexity of power-flow studies. These networks are no longer passive radial circuits; they are active, increasingly meshed, and characterized by bidirectional power flows, voltage-controlled nodes, and time-varying operating conditions [1, 2]. Accurate and computationally efficient power-flow methods are therefore essential for real-time monitoring, optimization, and control of modern distribution systems.

The classical power-flow problem is formulated as a set of nonlinear algebraic equations that relate the complex nodal voltages to the specified complex power injections. The solution of these equations has been addressed by a wide variety of numerical methods, each with its own advantages and limitations. Newton–Raphson (NR) and its variants remain the reference methods for transmission systems because of their quadratic convergence and robustness [3]. However, their application to distribution networks is complicated by the radial or weakly meshed topology, the high R/X ratio of the lines, and the large number of nodes, which can degrade the conditioning of the Jacobian matrix and increase the computational burden.

The specific characteristics of distribution networks have motivated the development of specialized power-flow methods. Among them, the backward/forward sweep (BFS) method is the most widely used because of its conceptual simplicity and low computational cost per iteration [4, 5, 6]. Its convergence properties, however, are closely tied to the radial topology of the network, and its extension to meshed configurations typically requires the use of compensation techniques or the solution of an inner loop [5, 7]. Other specialized methods include the current injection method, the graph-based method, and the triangular-matrix-based method [8, 9, 10, 11, 12].

1.2. Literature Review

The literature on power-flow methods for distribution networks is extensive. Comprehensive reviews can be found in [2, 13, 14, 15]. The main families of methods are briefly summarized below.

Newton-based methods. The Newton–Raphson method and its variants (fast-decoupled, current injection, and rectangular coordinates) exhibit quadratic convergence near the solution and are well established for transmission systems [3]. In distribution systems, however, their convergence can be sensitive to the initial guess, and the Jacobian matrix can become ill-conditioned when the R/X ratio is high or when the network is weakly meshed.

Backward/forward sweep methods. The BFS method exploits the radial topology of distribution networks to solve the power-flow equations through an iterative sequence of backward (current or power) and forward (voltage) sweeps [4, 5, 6]. The method is simple, robust, and computationally efficient. Its convergence has been analyzed in [4, 16, 17], where sufficient conditions have been derived in terms of the network parameters and the loading level. Nevertheless, the BFS method is essentially restricted to radial networks; meshed configurations require the introduction of compensation currents or the solution of a reduced-order system.

Holomorphic embedding methods. The holomorphic embedding load-flow method (HELM) provides a mathematically rigorous approach based on the analytic continuation of the power-flow equations [18]. It can provide information on the existence and uniqueness of the solution under suitable conditions, but its computational cost per iteration is higher than that of classical methods.

Successive approximation methods. Successive approximation methods, also known as fixed-point or Picard iterations, have been revisited in the context of distribution systems [19]. They are attractive because of their low computational cost per iteration and their ability to handle radial and meshed topologies under certain conditions. However, their convergence is not guaranteed in general, and a rigorous convergence analysis is often lacking.

Other specialized methods. Additional approaches include the rotational load-flow method [12], the modular power-flow method [20], the graph-based method [8], and the current injection method for meshed systems [21]. Each of these methods has been designed to address specific limitations of the classical methods.

Conceptual comparison of method families. For reference, the four main families discussed above can be positioned as follows. Newton-type methods offer quadratic local convergence but require the assembly and factorization of a Jacobian matrix at every iteration and provide no global convergence certificate. BFS methods have a very low per-iteration cost on radial networks but are topology-restricted and, in their classical form, lack a general convergence certificate. HELM provides existence and uniqueness information through the radius of convergence of a power series, at a higher per-iteration cost and with a different notion of certificate than a contraction radius. Successive-approximation (fixed-point) methods share the per-iteration structure of the method proposed here—one linear solve with a constant matrix—but are typically analyzed only empirically. The contribution of this work lies precisely in attaching an explicit Banach-based certificate, with a certified radius and computable error bounds, to a normalized fixed-point iteration of this last family. This comparison is conceptual and does not involve any numerical benchmarking.

1.3. Research Gap and Contributions

Despite the significant progress in power-flow methods for distribution systems, several gaps remain:

1. **Lack of a unified convergence certificate.** Most existing methods provide convergence conditions that are either topology-specific (e.g., BFS for radial networks) or based on empirical observations. To the best of our knowledge, and within the scope of the literature reviewed here, an explicit Banach-based certificate stated directly in normalized voltage coordinates and accompanied by computable a priori and a posteriori bounds is not commonly reported; we do not claim that no such certificate exists [22, 23].
2. **Limited theoretical guarantees.** Successive approximation methods are attractive for their simplicity, but their convergence is often established under restrictive assumptions. A rigorous analysis based on the Banach fixed-point theorem would provide sufficient conditions for existence, uniqueness, and convergence.
3. **Absence of a priori and a posteriori error bounds.** Most iterative power-flow methods provide only an empirical convergence criterion based on the difference between consecutive iterates. A priori and a posteriori error bounds with a direct theoretical interpretation are rarely available [24].

To address these gaps, this paper proposes a voltage-ratio fixed-point formulation for power-flow analysis in radial and meshed AC distribution networks. The main contributions of this work are the following:

- **Exact voltage-ratio representation.** The classical power-flow equations are recast exactly in terms of inverse squared-voltage magnitude variables and pairwise complex voltage-ratio variables. This representation is exact and does not introduce any approximation.
- **Compact normalized fixed-point mapping.** By normalizing the non-slack voltages with respect to the unique slack-bus voltage, a compact nodal fixed-point mapping is obtained. The nonlinearity of the mapping is confined to an element-wise reciprocal of the conjugated normalized voltage vector, which simplifies both the analysis and the numerical implementation.
- **Certified convergence via the Banach fixed-point theorem.** Sufficient conditions for the existence, uniqueness, and at-least-linear convergence of the fixed-point iteration are derived explicitly. The conditions depend only on the reduced nodal admittance matrix, the normalized complex power injections, the no-load voltage profile, and a certified contraction radius.
- **Topology-agnostic formulation and analysis.** The derivation of the fixed-point mapping and of the convergence certificate does not rely on radiality assumptions, parent–child relationships, or backward/forward sweep orderings. At the theoretical level, the analysis therefore applies to radial and meshed networks with a unique slack bus, provided that the reduced nodal admittance matrix is nonsingular. The numerical validation reported in this paper, however, is restricted to radial feeders.
- **A priori and a posteriori error bounds.** The contraction factor provides a priori and a posteriori error bounds with a direct theoretical interpretation. These bounds can be used to establish convergence criteria and to estimate the distance to the solution.
- **Numerical validation on radial test feeders.** The formulation and its convergence certificate are validated on the IEEE 33-bus and IEEE 69-bus radial distribution test feeders. The method converges to the same power-flow solution for all tested initial voltage magnitudes, and the computed voltage profiles agree with the classical benchmark results; the active power losses are consistent with them once the demand aggregation convention is taken into account. No meshed test system is analyzed in this work.

The proposed formulation is related to the successive approximation method of [19], but it differs in two important aspects. First, the voltage-ratio representation is exact and does not require the explicit inversion of the reduced nodal admittance matrix. Second, the convergence analysis is based on the Banach fixed-point theorem and provides a certified contraction radius, which is a stronger result than the empirical convergence conditions typically reported in the literature. It should be emphasized, however, that the per-iteration computational structure coincides with that of a normalized fixed-point (Picard) iteration: the contribution of this work is not a new iteration kernel, but (i) the exact voltage-ratio recasting that motivates the normalization and (ii) the Banach-based certificate attached to it. The voltage-ratio representation provides more than an algebraic rewriting: it identifies the inverse squared-voltage magnitude T_k and the ratios R_{km} as the natural variables in which the nonlinearity becomes an element-wise reciprocal, which is what makes the Banach estimate tractable and renders the topology-independence of the derivation manifest.

The proposed formulation also complements the classical BFS method [4, 16] and the Newton-based methods [3]. Unlike BFS, its derivation does not require a radial topology or compensation techniques. Unlike NR, it does not require the computation of the Jacobian matrix, and each iteration involves a single linear solve with a constant matrix. These are structural observations; no runtime comparison against NR or BFS is claimed in this paper.

1.4. Paper Organization

The remainder of this paper is organized as follows. Section 2 presents the voltage-ratio fixed-point formulation. Section 3 develops the convergence analysis using the Banach fixed-point theorem, including the self-mapping condition, the contraction condition, the convergence theorem, and the a priori and a posteriori error bounds. Section 4 discusses the computational implementation and the complexity of the main steps. Section 5 reports the numerical results on the IEEE 33-bus and IEEE 69-bus radial distribution test feeders, together with an

explicit discussion of the scope and limitations of the present validation. Finally, Section 6 summarizes the main conclusions and outlines directions for future work.

2. Voltage-Ratio Fixed-Point Formulation

Consider a balanced AC network composed of the set of buses $\mathcal{N} = \{0, 1, \ldots, n\}$, where bus 0 is the unique slack bus and $\mathcal{L} = \mathcal{N} \setminus \{0\}$ denotes the set of non-slack buses. The formulation is stated for a general network that may have either a radial or a meshed topology. The complex voltage at the slack bus is assumed to be known, real, and denoted by $V_0 = |V_0|\angle 0$. All non-slack bus voltages are assumed to be nonzero, i.e., $V_k \neq 0$ for all $k \in \mathcal{L}$; the implications of this assumption are discussed in Remark 1 and in Section 5.5.

For each non-slack bus $k \in \mathcal{L}$, the conventional nodal complex power-flow equation can be written as

$$S_k^* = V_k^* \sum_{m \in \mathcal{N}} Y_{km} V_m, \qquad \forall k \in \mathcal{L}, \tag{1}$$

where $S_k = P_k + jQ_k$ is the specified net complex power injection (generation minus load), V_k is the complex nodal voltage, and Y_{km} denotes the (k, m) entry of the nodal admittance matrix $\mathbf{Y}$.

To obtain an alternative representation of the power-flow equations, define the inverse squared-voltage magnitude variable

$$T_k = \frac{1}{|V_k|^2}, \qquad \forall k \in \mathcal{N}, \tag{2}$$

together with the pairwise complex voltage-ratio variable

$$R_{km} = \frac{V_m}{V_k}, \qquad \forall (k, m) \in \mathcal{N} \times \mathcal{N}. \tag{3}$$

Multiplying (1) by T_k and using

$$T_k V_k^* = \frac{V_k^*}{|V_k|^2} = \frac{1}{V_k}, \tag{4}$$

yields

$$S_k^* T_k = \sum_{m \in \mathcal{N}} Y_{km} \frac{V_m}{V_k}. \tag{5}$$

Therefore, the power-flow equations admit the exact voltage-ratio representation

$$S_k^* T_k = \sum_{m \in \mathcal{N}} Y_{km} R_{km}, \qquad \forall k \in \mathcal{L}. \tag{6}$$

The transformed variables satisfy the identities

$$R_{kk} = 1, \qquad \forall k \in \mathcal{N}, \tag{7}$$

$$R_{km} R_{mn} = R_{kn}, \qquad \forall k, m, n \in \mathcal{N}, \tag{8}$$

and

$$R_{mk} = \frac{1}{R_{km}}. \tag{9}$$

Moreover, the squared magnitude of the voltage ratio satisfies

$$|R_{km}|^2 = \frac{|V_m|^2}{|V_k|^2} = \frac{T_k}{T_m}, \tag{10}$$

or equivalently,

$$T_m |R_{km}|^2 = T_k. \tag{11}$$

Although (6) provides an exact representation of the power-flow equations, explicitly introducing all pairwise voltage ratios R_{km} is unnecessary. A compact nodal representation can be obtained by normalizing all non-slack voltages with respect to the unique slack voltage.

Define

$$q_k = \frac{V_k}{V_0}, \qquad \forall k \in \mathcal{L}, \tag{12}$$

and the normalized complex power injection

$$\sigma_k = \frac{S_k}{|V_0|^2}, \qquad \forall k \in \mathcal{L}. \tag{13}$$

Note that $\sigma_k^* = S_k^* T_0$, where $T_0 = 1/|V_0|^2$.

Consequently,

$$V_k = V_0 q_k, \tag{14}$$

and the transformed variable T_k can be recovered as

$$T_k = \frac{1}{|V_0|^2 |q_k|^2}. \tag{15}$$

Substitution of (14) into (1) gives

$$\sigma_k^* = q_k^* \left(Y_{k0} + \sum_{m \in \mathcal{L}} Y_{km} q_m \right), \qquad \forall k \in \mathcal{L}, \tag{16}$$

where the assumption $V_0 = |V_0| \angle 0$ has been used to set $V_0^*/V_0 = 1$.

Assuming $q_k \neq 0$, division by q_k^* results in

$$\sum_{m \in \mathcal{L}} Y_{km} q_m = \frac{\sigma_k^*}{q_k^*} - Y_{k0}, \qquad \forall k \in \mathcal{L}. \tag{17}$$

Let $\mathbf{q} \in \mathbb{C}^n$ collect the normalized voltages of all non-slack buses, and partition the nodal admittance matrix as

$$\mathbf{Y} = \begin{bmatrix} Y_{00} & \mathbf{y}_{0L}^{\mathsf{T}} \\ \mathbf{y}_{L0} & \mathbf{Y}_{LL} \end{bmatrix}. \tag{18}$$

Additionally, define

$$\mathbf{D}_{\boldsymbol{\sigma}^*} = \operatorname{diag}\left(\sigma_1^*, \sigma_2^*, \ldots, \sigma_n^*\right). \tag{19}$$

The complete set of non-slack power-flow equations can then be expressed compactly as

$$\mathbf{Y}_{LL}\mathbf{q} = \mathbf{D}_{\boldsymbol{\sigma}^*} \left(\mathbf{q}^*\right)^{\circ(-1)} - \mathbf{y}_{L0}, \tag{20}$$

where $(\cdot)^{\circ(-1)}$ denotes the element-wise reciprocal operation, and $|\mathbf{A}|$, for a matrix $\mathbf{A}$, denotes the element-wise absolute value. Throughout this paper, the inequality $|\mathbf{A}\mathbf{x}| \leq |\mathbf{A}|\,|\mathbf{x}|$ is understood component-wise and is the basis of all majorizations used in Section 3.

Remark 1

The element-wise reciprocal in (20) requires $q_k \neq 0$ for all $k \in \mathcal{L}$. Inside the certified ball $\mathcal{D}_\rho$ introduced in Section 3, this requirement is guaranteed by the condition $\rho < \min_{k \in \mathcal{L}} |q_k^0|$ (see (35)), which ensures that no component of $\mathbf{q}$ vanishes in $\mathcal{D}_\rho$. Outside the certified region, however, no such guarantee exists: as $|q_k| \to 0$, the term σ_k^*/q_k^* grows without bound, and the mapping may become undefined or numerically unstable. Consequently, the method in its present form is not intended for operating points at or beyond the voltage-collapse point; the certificate excludes such points by construction. Possible safeguards for operation close to this regime—such as step damping, trust-region truncation, or a fallback to a damped Newton step—are discussed in Section 5.5 but are not implemented or tested in this work.

Remark 2
The partition (18) and the subsequent developments assume that $\mathbf{Y}_{LL}$ is nonsingular. For a connected network with a unique slack bus and passive shunt elements, this is the typical case. The assumption may fail, however, in the presence of (i) islanded sub-networks without their own slack bus, (ii) ideal (lossless, zero-admittance) branches that leave voltage differences unobservable, or (iii) certain singular shunt configurations. Nonsingularity of $\mathbf{Y}_{LL}$ is therefore stated as an explicit assumption of Theorem 1, and not as an automatic consequence of connectivity.

Equation (20) naturally defines the following fixed-point mapping:

$$\mathbf{q}^{(t+1)} = \mathbf{Y}_{LL}^{-1}\left[\mathbf{D}_{\boldsymbol{\sigma}^*}\left(\mathbf{q}^{*(t)}\right)^{\circ(-1)} - \mathbf{y}_{L0}\right]. \tag{21}$$

For numerical implementation, the explicit computation of $\mathbf{Y}_{LL}^{-1}$ is unnecessary. Instead, at iteration $t+1$, the following complex linear system can be solved:

$$\mathbf{Y}_{LL}\mathbf{q}^{(t+1)} = \mathbf{D}_{\boldsymbol{\sigma}^*}\left(\mathbf{q}^{*(t)}\right)^{\circ(-1)} - \mathbf{y}_{L0}. \tag{22}$$

Starting from an initial voltage profile $\mathbf{q}^{(0)}$, the iterative procedure is repeated until

$$\left\|\mathbf{q}^{(t+1)} - \mathbf{q}^{(t)}\right\|_{\infty} \leq \varepsilon, \tag{23}$$

where $\varepsilon > 0$ is a prescribed convergence tolerance. Once convergence is achieved, the physical nodal voltages are recovered according to

$$\mathbf{V}_L = V_0\mathbf{q}, \tag{24}$$

whereas the inverse squared-voltage variables follow from

$$T_k = \frac{1}{|V_0|^2|q_k|^2}, \qquad \forall k \in \mathcal{L}. \tag{25}$$

An important feature of (22) is that its derivation does not require a particular network topology, a parent–child relationship, or a backward/forward sweep ordering. Consequently, the same formulation applies, at the theoretical level, to both radial and meshed networks containing a unique slack bus, provided that the reduced nodal admittance matrix $\mathbf{Y}_{LL}$ is nonsingular (see Remark 2). It should be emphasized that this topology-agnostic character is a property of the derivation and of the convergence analysis; it is not, in this work, accompanied by a numerical validation on meshed test systems.

3. Convergence Analysis via the Banach Fixed-Point Theorem

The fixed-point representation introduced in (21) enables the establishment of sufficient conditions for the existence, uniqueness, and convergence of the power-flow solution. In this section, these conditions are derived using the Banach fixed-point theorem. The derivation is purely algebraic and does not invoke radiality assumptions; it therefore applies, at the theoretical level, to both radial and meshed networks with a unique slack bus.

For convenience, define the fixed-point mapping $\mathcal{F} : \mathbb{C}^n \to \mathbb{C}^n$ as

$$\mathcal{F}(\mathbf{q}) = \mathbf{Y}_{LL}^{-1}\left[\mathbf{D}_{\boldsymbol{\sigma}^*}\left(\mathbf{q}^*\right)^{\circ(-1)} - \mathbf{y}_{L0}\right], \tag{26}$$

such that the proposed iterative procedure can be expressed as

$$\mathbf{q}^{(t+1)} = \mathcal{F}\left(\mathbf{q}^{(t)}\right). \tag{27}$$

The nonlinear dependence of $\mathcal{F}$ on $\mathbf{q}$ is exclusively associated with the element-wise reciprocal of the conjugated normalized voltage vector.

3.0.1. No-Load Operating Point Consider first the no-load condition

$$\boldsymbol{\sigma} = \mathbf{0}. \tag{28}$$

Under this condition, (20) reduces to

$$\mathbf{Y}_{LL}\mathbf{q}^0 = -\mathbf{y}_{L0}, \tag{29}$$

and therefore the corresponding normalized no-load voltage profile is

$$\mathbf{q}^0 = -\mathbf{Y}_{LL}^{-1}\mathbf{y}_{L0}. \tag{30}$$

The vector $\mathbf{q}^0$ provides a natural center around which a convergence region can be constructed.
For a given scalar $\rho > 0$, define the closed set

$$\mathcal{D}_\rho = \left\{\mathbf{q} \in \mathbb{C}^n : \left\|\mathbf{q} - \mathbf{q}^0\right\|_\infty \le \rho\right\}. \tag{31}$$

Since $\mathbb{C}^n$ equipped with the infinity norm is a complete metric space, the closed subset $\mathcal{D}_\rho$ is also complete.
For every $\mathbf{q} \in \mathcal{D}_\rho$, the reverse triangle inequality gives

$$|q_k| \ge |q_k^0| - |q_k - q_k^0| \ge |q_k^0| - \rho. \tag{32}$$

Define

$$r_k(\rho) = |q_k^0| - \rho, \qquad \forall k \in \mathcal{L}, \tag{33}$$

and collect these quantities in the vector

$$\mathbf{r}(\rho) = \begin{bmatrix} r_1(\rho) & \cdots & r_n(\rho) \end{bmatrix}^{\mathsf{T}}. \tag{34}$$

The radius ρ is restricted according to

$$0 < \rho < \min_{k\in\mathcal{L}} |q_k^0|, \tag{35}$$

which guarantees

$$r_k(\rho) > 0, \qquad \forall k \in \mathcal{L}. \tag{36}$$

Consequently, no component of $\mathbf{q}$ can vanish inside $\mathcal{D}_\rho$, and the mapping (26) is well defined throughout this set.

3.0.2. Self-Mapping Condition The first requirement of the Banach fixed-point theorem is that $\mathcal{F}$ maps $\mathcal{D}_\rho$ into itself.
Using (30), the mapping (26) can be equivalently written as

$$\mathcal{F}(\mathbf{q}) = \mathbf{q}^0 + \mathbf{Y}_{LL}^{-1}\mathbf{D}_{\boldsymbol{\sigma}^*}\left(\mathbf{q}^*\right)^{\circ(-1)}. \tag{37}$$

Therefore,

$$\mathcal{F}(\mathbf{q}) - \mathbf{q}^0 = \mathbf{Y}_{LL}^{-1}\mathbf{D}_{\boldsymbol{\sigma}^*}\left(\mathbf{q}^*\right)^{\circ(-1)}. \tag{38}$$

Taking component-wise absolute values yields

$$\left|\mathcal{F}(\mathbf{q}) - \mathbf{q}^0\right| \le \left|\mathbf{Y}_{LL}^{-1}\right| |\boldsymbol{\sigma}| \oslash |\mathbf{q}|, \tag{39}$$

where $\oslash$ denotes element-wise division.
From (32),

$$|\mathbf{q}| \ge \mathbf{r}(\rho), \tag{40}$$

and hence

$$\left|\mathcal{F}(\mathbf{q}) - \mathbf{q}^0\right| \le \left|\mathbf{Y}_{LL}^{-1}\right| \left(|\boldsymbol{\sigma}| \oslash \mathbf{r}(\rho)\right). \tag{41}$$

Taking the infinity norm on both sides gives

$$\left\|\mathcal{F}(\mathbf{q}) - \mathbf{q}^0\right\|_\infty \le \left\|\left|\mathbf{Y}_{LL}^{-1}\right| \left(|\boldsymbol{\sigma}| \oslash \mathbf{r}(\rho)\right)\right\|_\infty. \tag{42}$$

Therefore, a sufficient condition for $\mathcal{F}(\mathcal{D}_\rho) \subseteq \mathcal{D}_\rho$ is

$$\left\|\left|\mathbf{Y}_{LL}^{-1}\right| \left(|\boldsymbol{\sigma}| \oslash \mathbf{r}(\rho)\right)\right\|_\infty \le \rho. \tag{43}$$

3.0.3. Contraction Condition The second requirement is to establish that $\mathcal{F}$ is a contraction on $\mathcal{D}_\rho$. Consider any two normalized voltage vectors $\mathbf{q}, \mathbf{p} \in \mathcal{D}_\rho$. From (26),

$$\mathcal{F}(\mathbf{q}) - \mathcal{F}(\mathbf{p}) = \mathbf{Y}_{LL}^{-1}\mathbf{D}_{\boldsymbol{\sigma}^*}\left[(\mathbf{q}^*)^{\circ(-1)} - (\mathbf{p}^*)^{\circ(-1)}\right]. \tag{44}$$

For each component $k \in \mathcal{L}$,

$$\frac{1}{q_k^*} - \frac{1}{p_k^*} = \frac{p_k^* - q_k^*}{q_k^* p_k^*}. \tag{45}$$

Consequently,

$$\left|\frac{1}{q_k^*} - \frac{1}{p_k^*}\right| = \frac{|q_k - p_k|}{|q_k||p_k|}. \tag{46}$$

Since $\mathbf{q}, \mathbf{p} \in \mathcal{D}_\rho$,

$$|q_k| \geq r_k(\rho), \qquad |p_k| \geq r_k(\rho), \tag{47}$$

and thus

$$\left|\frac{1}{q_k^*} - \frac{1}{p_k^*}\right| \leq \frac{|q_k - p_k|}{r_k^2(\rho)}. \tag{48}$$

Using (48) in (44) gives

$$|\mathcal{F}(\mathbf{q}) - \mathcal{F}(\mathbf{p})| \leq \left|\mathbf{Y}_{LL}^{-1}\right| \operatorname{diag}\left(\frac{|\sigma_1|}{r_1^2(\rho)}, \ldots, \frac{|\sigma_n|}{r_n^2(\rho)}\right) |\mathbf{q} - \mathbf{p}|. \tag{49}$$

Taking the infinity norm results in

$$\|\mathcal{F}(\mathbf{q}) - \mathcal{F}(\mathbf{p})\|_\infty \leq \alpha(\rho)\, \|\mathbf{q} - \mathbf{p}\|_\infty, \tag{50}$$

where the contraction factor is defined as

$$\alpha(\rho) = \left\| \left|\mathbf{Y}_{LL}^{-1}\right| \operatorname{diag}\left(|\boldsymbol{\sigma}| \oslash \mathbf{r}^{\circ 2}(\rho)\right) \right\|_\infty. \tag{51}$$

Therefore, $\mathcal{F}$ is a contraction on $\mathcal{D}_\rho$ whenever

$$\alpha(\rho) < 1. \tag{52}$$

3.0.4. Convergence Theorem The previous results lead directly to the following convergence theorem.

Theorem 1 (Convergence of the normalized voltage fixed-point iteration)
Let $\mathbf{Y}_{LL}$ be nonsingular (see Remark 2 for the cases in which this assumption may fail) and let

$$\mathbf{q}^0 = -\mathbf{Y}_{LL}^{-1}\mathbf{y}_{L0}. \tag{53}$$

Consider a radius ρ satisfying

$$0 < \rho < \min_{k \in \mathcal{L}} |q_k^0|, \tag{54}$$

and define

$$r_k(\rho) = |q_k^0| - \rho. \tag{55}$$

If the following two conditions hold:

$$\left\| \left|\mathbf{Y}_{LL}^{-1}\right| (|\boldsymbol{\sigma}| \oslash \mathbf{r}(\rho)) \right\|_\infty \leq \rho, \tag{56}$$

and

$$\left\| \left|\mathbf{Y}_{LL}^{-1}\right| \operatorname{diag}\left(|\boldsymbol{\sigma}| \oslash \mathbf{r}^{\circ 2}(\rho)\right) \right\|_\infty < 1, \tag{57}$$

then the mapping $\mathcal{F}$ defined in (26) has a unique fixed point $\mathbf{q}^\star$ *within* $\mathcal{D}_\rho$. Moreover, for every initial point

$$\mathbf{q}^{(0)} \in \mathcal{D}_\rho, \tag{58}$$

the sequence generated by

$$\mathbf{q}^{(t+1)} = \mathcal{F}\left(\mathbf{q}^{(t)}\right) \tag{59}$$

converges to $\mathbf{q}^\star$.

The theorem establishes existence and uniqueness of the fixed point inside the certified ball $\mathcal{D}_\rho$, and the convergence of the iteration from any starting point in that ball. It does not establish global uniqueness of the power-flow solution, nor does it establish convergence from starting points outside $\mathcal{D}_\rho$; those are empirical questions addressed in Section 5.

Proof. Condition (56), together with (42), guarantees that

$$\mathcal{F}(\mathcal{D}_\rho) \subseteq \mathcal{D}_\rho. \tag{60}$$

Moreover, condition (57) and (50) imply that there exists a constant $\alpha(\rho) < 1$ such that

$$\|\mathcal{F}(\mathbf{q}) - \mathcal{F}(\mathbf{p})\|_\infty \leq \alpha(\rho)\, \|\mathbf{q} - \mathbf{p}\|_\infty\,, \tag{61}$$

for all $\mathbf{q}, \mathbf{p} \in \mathcal{D}_\rho$. Hence, $\mathcal{F}$ is a contraction mapping from the complete metric space $\mathcal{D}_\rho$ into itself. By the Banach fixed-point theorem, $\mathcal{F}$ admits a unique fixed point $\mathbf{q}^\star \in \mathcal{D}_\rho$, and the fixed-point iteration converges to $\mathbf{q}^\star$ from any initial condition belonging to $\mathcal{D}_\rho$. Since a fixed point of $\mathcal{F}$ satisfies (20), $\mathbf{q}^\star$ also satisfies the original AC power-flow equations after recovering the physical voltages through $\mathbf{V}_L = V_0\mathbf{q}^\star$. □

3.0.5. Convergence Rate and Error Bounds The Banach fixed-point theorem additionally provides an upper bound on the convergence rate. For $\alpha(\rho) < 1$,

$$\left\|\mathbf{q}^{(t)} - \mathbf{q}^\star\right\|_\infty \leq \alpha^t(\rho) \left\|\mathbf{q}^{(0)} - \mathbf{q}^\star\right\|_\infty. \tag{62}$$

Therefore, the proposed iteration is guaranteed to converge at least linearly inside the certified contraction region.

Since $\mathbf{q}^\star$ is unknown during the iterative solution, (62) is a rate bound rather than a directly computable error bound. A computable a priori bound can be obtained by noting that, for $\mathbf{q}^{(0)}, \mathbf{q}^\star \in \mathcal{D}_\rho$, one has $\|\mathbf{q}^{(0)} - \mathbf{q}^\star\|_\infty \leq 2\rho$, which yields

$$\left\|\mathbf{q}^{(t)} - \mathbf{q}^\star\right\|_\infty \leq 2\rho\, \alpha^t(\rho). \tag{63}$$

This bound depends only on the certified radius and the contraction factor, both of which are available once the certificate has been evaluated.

A tighter, a posteriori error bound can be obtained exclusively from two consecutive iterates as

$$\left\|\mathbf{q}^{(t)} - \mathbf{q}^\star\right\|_\infty \leq \frac{\alpha(\rho)}{1-\alpha(\rho)} \left\|\mathbf{q}^{(t)} - \mathbf{q}^{(t-1)}\right\|_\infty. \tag{64}$$

This expression provides a convergence criterion with a direct theoretical interpretation and is the practically useful bound in the implementation. In particular, if the practical stopping rule (23) is used with tolerance ε, then, whenever the iterate lies in $\mathcal{D}_\rho$ and $\alpha(\rho) < 1$, the certified error satisfies $\|\mathbf{q}^{(t)} - \mathbf{q}^\star\|_\infty \leq \frac{\alpha(\rho)}{1-\alpha(\rho)}\varepsilon$.

3.0.6. Simplified Sufficient Condition A more compact, although potentially more conservative, convergence condition can be obtained by defining

$$r_{\min}(\rho) = \min_{k\in\mathcal{L}} |q_k^0| - \rho. \tag{65}$$

Since

$$|q_k| \geq r_{\min}(\rho), \qquad \forall k \in \mathcal{L}, \tag{66}$$

the contraction factor can be bounded according to

$$\alpha(\rho) \leq \frac{\left\|\mathbf{Y}_{LL}^{-1}\mathbf{D}_{\boldsymbol{\sigma}^*}\right\|_\infty}{r_{\min}^2(\rho)}. \tag{67}$$

Consequently, the readily computable condition

$$\frac{\left\|\mathbf{Y}_{LL}^{-1}\mathbf{D}_{\boldsymbol{\sigma}^*}\right\|_\infty}{\left(\min\limits_{k\in\mathcal{L}}|q_k^0| - \rho\right)^2} < 1 \tag{68}$$

is sufficient to establish contractivity. Nevertheless, (51) is generally preferable because it preserves the bus-dependent information contained in $|\sigma_k|$ and $r_k(\rho)$ and is therefore expected to provide a less conservative certificate.

3.0.7. Discussion The conditions derived above provide an explicit convergence certificate that depends exclusively on the reduced nodal admittance matrix, the normalized complex power injections, the no-load voltage profile, and the selected radius ρ. In particular, no assumption concerning a radial network structure, branch ordering, parent–child relationships, or backward/forward sweeps is required. At the theoretical level, the same convergence analysis therefore applies to radial and meshed networks with a unique slack bus, provided that $\mathbf{Y}_{LL}$ is nonsingular.

It is important to emphasize that conditions (56)–(57) are sufficient rather than necessary. Therefore, failure to satisfy the proposed certificate does not imply that the power-flow solution does not exist or that the fixed-point iteration necessarily diverges. Instead, satisfaction of these conditions guarantees the existence of a unique solution within $\mathcal{D}_\rho$ and convergence of the iterative procedure from any initial point inside the certified region.

Sources of conservatism. The certificate is conservative for three reasons. First, it uses the infinity norm and the element-wise absolute-value majorization of $\mathbf{Y}_{LL}^{-1}$, which discard sign and phase information. Second, it bounds the reciprocal nonlinearity by a worst-case Lipschitz constant over the entire ball $\mathcal{D}_\rho$, whereas the actual local Lipschitz constant near the solution is typically smaller. Third, the self-mapping condition is stronger than what is strictly needed to establish convergence. As a consequence, the certified radius is expected to underestimate the empirical basin of attraction. This is the expected behavior of a sufficient condition of this kind, and it is consistent with the numerical observations reported in Section 5, where the iteration converges from initial points that lie outside any certified ball that could be constructed from the present bounds. A quantitative parametric study of the gap between the certified radius and the empirical basin of attraction is not included in this work and is identified as future work in Section 5.5.

Choice of the radius. The certified radius ρ is not unique. For a given system, the sharpest certificate is obtained by maximizing ρ over the admissible interval $(0, \min_{k\in\mathcal{L}}|q_k^0|)$ subject to conditions (56)–(57). The simplified condition (68) provides a cheaper but more conservative alternative, and the bus-dependent condition (57) is generally preferable because it preserves the bus-dependent information contained in $|\sigma_k|$ and $r_k(\rho)$.

4. Computational Implementation and Complexity

This section describes the computational structure of one iteration of the proposed method and provides a formal complexity analysis of its main steps. The purpose is twofold: to make the implementation reproducible and to allow a fair assessment of the computational burden of the method relative to established sparse solvers, as requested by the reviewers.

Per-iteration cost. At each iteration, the right-hand side of (22) is formed by (i) the element-wise reciprocal of $\mathbf{q}^{*(t)}$, which costs $O(n)$ operations; (ii) the element-wise product with the diagonal matrix $\mathbf{D}_{\boldsymbol{\sigma}^*}$, which costs

$O(n)$; and (iii) the subtraction of $\mathbf{y}_{L0}$, which costs $O(n)$. The resulting linear system is then solved with the fixed matrix $\mathbf{Y}_{LL}$. Since $\mathbf{Y}_{LL}$ is constant across iterations, its factorization can be computed once and reused for all subsequent iterations, so that each iteration reduces to one forward and one backward substitution. If $\mathbf{Y}_{LL}$ is stored and factorized in sparse form, the per-iteration cost is $O(\mathrm{nnz}(L+U))$, where L and U are the factors of $\mathbf{Y}_{LL}$; this is the dominant cost of each iteration.

Reuse of the factorization. The fact that $\mathbf{Y}_{LL}$ is constant is a structural advantage of the proposed iteration over Newton-type methods, which must reassemble and refactorize the Jacobian matrix at every iteration. In the proposed method, the factorization is performed once, before the iteration starts, and the per-iteration cost is therefore dominated by the triangular solves. This observation is structural and does not, by itself, establish a runtime advantage over any particular method; establishing such an advantage would require a same-platform benchmarking study, which is not performed in this work.

Memory requirements. The method requires storage of $\mathbf{Y}_{LL}$ and of its factorization, which, for a sparse implementation, scales as $O(\mathrm{nnz}(\mathbf{Y}_{LL}))$ plus the fill-in introduced by the factorization. No dense $n \times n$ matrix is required. The vectors $\mathbf{q}^{(t)}$, $\boldsymbol{\sigma}$, $\mathbf{y}_{L0}$, and the intermediate right-hand side each require $O(n)$ storage.

Cost of evaluating the certificate. The self-mapping condition (56) and the contraction condition (57) involve the absolute-value matrix $|\mathbf{Y}_{LL}^{-1}|$. Forming $|\mathbf{Y}_{LL}^{-1}|$ explicitly costs $O(n^3)$ operations and $O(n^2)$ storage, since $\mathbf{Y}_{LL}^{-1}$ is generally dense even when $\mathbf{Y}_{LL}$ is sparse. Once $|\mathbf{Y}_{LL}^{-1}|$ is available, the evaluation of (56) requires one matrix–vector product with $|\mathbf{Y}_{LL}^{-1}|$, costing $O(n^2)$; the evaluation of (57) requires either the formation of the matrix product $|\mathbf{Y}_{LL}^{-1}|\,\mathrm{diag}(|\boldsymbol{\sigma}| \oslash \mathbf{r}^{\circ 2}(\rho))$ or the computation of its maximum absolute row sum, both costing $O(n^2)$. The certificate is therefore an offline or design-time tool in the present implementation: it is evaluated once, on a grid of admissible radii ρ, and its cost is not included in the reported iteration counts. A cheaper but more conservative alternative is the simplified condition (68), which only requires $\|\mathbf{Y}_{LL}^{-1}\mathbf{D}_{\boldsymbol{\sigma}^*}\|_\infty$ and can be evaluated with one matrix–vector product once $\mathbf{Y}_{LL}^{-1}$ is known.

Procedure for computing the certificate. For a given test system, the certificate can be computed as follows: (i) form $\mathbf{Y}_{LL}$, $\mathbf{y}_{L0}$, and $\boldsymbol{\sigma}$; (ii) compute $\mathbf{q}^0 = -\mathbf{Y}_{LL}^{-1}\mathbf{y}_{L0}$ and the bound $\rho_{\max} = \min_{k\in\mathcal{L}} |q_k^0|$; (iii) form $|\mathbf{Y}_{LL}^{-1}|$; (iv) for a grid of admissible radii $\rho \in (0, \rho_{\max})$, evaluate (56) and (57); (v) select the largest ρ for which both conditions hold, and report the corresponding contraction factor $\alpha(\rho)$. This procedure is fully reproducible and does not require any power-flow simulation. In the present work, this procedure is described for completeness but is not applied to the test feeders; the numerical evaluation of the certificate on the test systems is identified as future work in Section 5.5.

Implementation used in this paper. The simulations reported in Section 5 were performed with a dense MATLAB implementation. A sparse implementation is expected to be beneficial for large systems, but it has not been benchmarked in this work.

5. Test Feeders and Numerical Results

This section evaluates the proposed voltage-ratio fixed-point power-flow formulation on two standard distribution test feeders: the IEEE 33-bus radial distribution network and the IEEE 69-bus radial distribution network. Both test feeders are radial; no meshed test system is analyzed in this work. For each feeder, the demand is kept fixed while the initial voltage magnitude is swept from 0.1 to 1.9 p.u. in steps of 0.1 p.u. The sweep is performed with a flat initial angle, i.e., all non-slack buses are initialized with zero angle; angle initialization, load stress, and ill-conditioned cases are not examined in this work. The following quantities are reported for each case: the number of iterations required for convergence, the minimum and maximum final voltage magnitudes, the total active power loss, and the total reactive power loss.

All simulations were implemented in a dense MATLAB implementation on a standard desktop computer. The convergence tolerance was set to $\varepsilon = 10^{-12}$ in the infinity norm, and the maximum number of iterations was limited to 5000. The slack-bus voltage was taken as $V_0 = 1.0\angle 0^\circ$ p.u., consistent with the assumption adopted in Section 2. Voltage magnitudes are reported to six decimal places (p.u.); active and reactive power losses are reported to four decimal places (kW and kVAr); iteration counts are integers.

Table 1. IEEE 33-bus feeder: convergence results and power losses as a function of the initial voltage magnitude.

Case	$\lvert q^{(0)}\rvert$ (p.u.)	Conv.	$\min \lvert V\rvert$ (p.u.)	$\max \lvert V\rvert$ (p.u.)	P_{loss} (kW)	Q_{loss} (kVAr)	Iter.
1	0.1	Yes	0.903778	1.000000	210.9876	143.1284	14
2	0.2	Yes	0.903778	1.000000	210.9876	143.1284	13
3	0.3	Yes	0.903778	1.000000	210.9876	143.1284	13
4	0.4	Yes	0.903778	1.000000	210.9876	143.1284	13
5	0.5	Yes	0.903778	1.000000	210.9876	143.1284	13
6	0.6	Yes	0.903778	1.000000	210.9876	143.1284	12
7	0.7	Yes	0.903778	1.000000	210.9876	143.1284	12
8	0.8	Yes	0.903778	1.000000	210.9876	143.1284	12
9	0.9	Yes	0.903778	1.000000	210.9876	143.1284	11
10	1.0	Yes	0.903778	1.000000	210.9876	143.1284	12
11	1.1	Yes	0.903778	1.000000	210.9876	143.1284	12
12	1.2	Yes	0.903778	1.000000	210.9876	143.1284	12
13	1.3	Yes	0.903778	1.000000	210.9876	143.1284	12
14	1.4	Yes	0.903778	1.000000	210.9876	143.1284	12
15	1.5	Yes	0.903778	1.000000	210.9876	143.1284	12
16	1.6	Yes	0.903778	1.000000	210.9876	143.1284	12
17	1.7	Yes	0.903778	1.000000	210.9876	143.1284	12
18	1.8	Yes	0.903778	1.000000	210.9876	143.1284	12
19	1.9	Yes	0.903778	1.000000	210.9876	143.1284	12

5.1. IEEE 33-Bus Radial Distribution Network

The IEEE 33-bus radial distribution network is a standard benchmark for distribution power-flow studies [25]. It consists of 33 buses, 32 branches, and a single slack bus at bus 1. The nominal voltage is 12.66 kV, and the base power is 1 MVA. The total connected load is 3.715 MW and 2.300 MVAr. The branch impedances and bus demands are taken from the classical data set reported by Baran and Wu [25], which is widely used for benchmarking power-flow methods for distribution systems [13, 14, 15]. In the present implementation, the demand is assigned to the receiving bus of each branch; this aggregation convention is stated explicitly because it explains the small difference between the total active power loss reported below and the classical value of [25] (see Section 5.3).

Table 1 reports the convergence results and power losses for the IEEE 33-bus feeder as a function of the initial voltage magnitude $|q^{(0)}|$. The fixed-point iteration converged for all tested initial values, with the number of iterations ranging from 14 (at $|q^{(0)}| = 0.1$ p.u.) to 11–12 for the remaining cases. The final voltage magnitudes, active power loss, and reactive power loss are identical across all cases, which is consistent with the convergence of all runs to the same solution.

The total active power loss is 210.9876 kW, and the total reactive power loss is 143.1284 kVAr. The minimum voltage magnitude is 0.903778 p.u. at bus 18, which is within the acceptable range of 0.90–1.10 p.u. The overall maximum voltage magnitude is 1.000000 p.u. at the slack bus. Among the non-slack buses, the maximum voltage magnitude is 0.997014 p.u. at bus 2, which is consistent with the physical solution.

Fig. 1 shows the voltage profile for the reference case ($|q^{(0)}| = 1.0$ p.u.). The voltage magnitudes decrease monotonically from the slack bus to the end of the feeder, reaching a minimum of 0.903778 p.u. at bus 18. The voltage angles are negative and increase in magnitude toward the end of the feeder, reflecting the power flow from the slack bus to the loads.

Fig. 2 shows the convergence behavior as a function of the initial voltage magnitude. The number of iterations decreases from 14 at $|q^{(0)}| = 0.1$ p.u. to 11–12 for the remaining cases, which is consistent with the contraction property established in Theorem 1 for initial points inside the certified region. The final voltage envelope and the total power losses are invariant across all cases, which is consistent with the convergence of all runs to the same solution.

Table 2 reports the per-branch power losses for the reference case. The largest losses occur on branches 2 (52.08 kW), 5 (38.57 kW), and 27 (11.31 kW), which correspond to the sections of the feeder that carry the largest

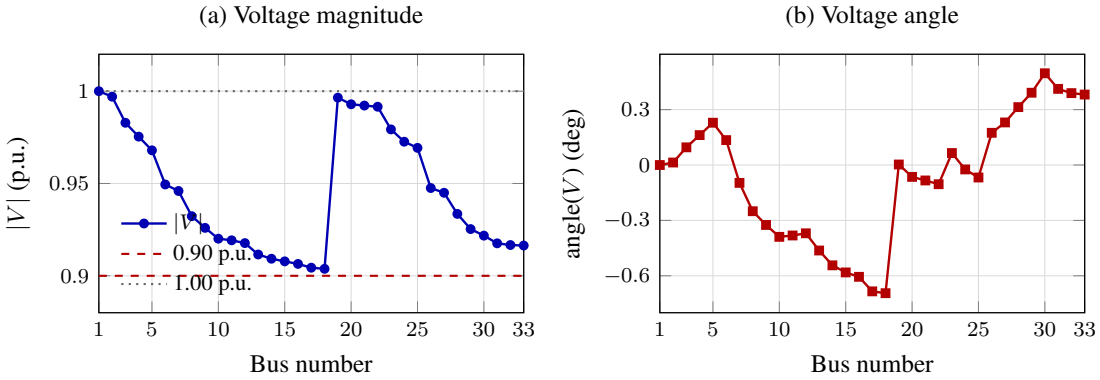

Figure 1. IEEE 33-bus voltage profile for the reference case ($|q^{(0)}| = 1.0$ p.u.).

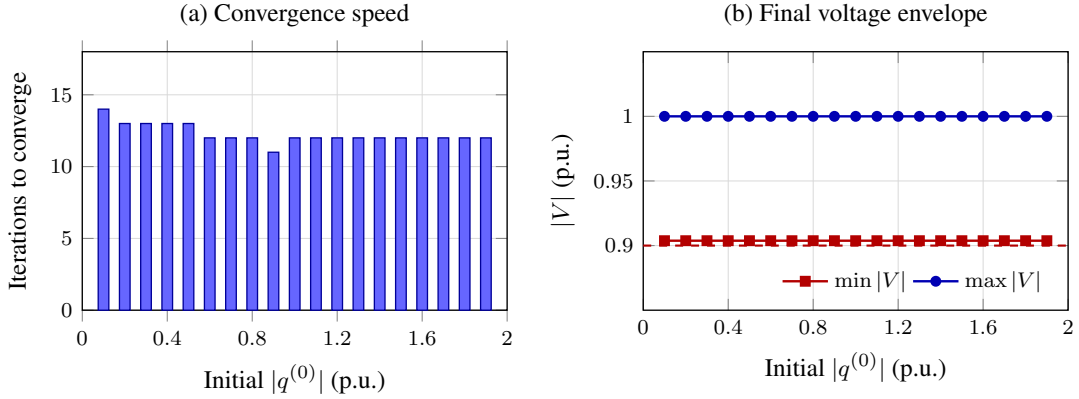

Figure 2. IEEE 33-bus feeder: (a) iterations to converge and (b) final voltage envelope, as functions of the initial voltage magnitude.

currents. The sum of the per-branch active power losses in Table 2 equals the total of 210.9876 kW reported in Table 1, and the same holds for the reactive power losses.

5.2. IEEE 69-Bus Radial Distribution Network

The IEEE 69-bus radial distribution network is a larger benchmark with 69 buses, 68 branches, and a single slack bus at bus 1. The nominal voltage is 12.66 kV, and the base power is 1 MVA. The total connected load is 3.8907 MW and 2.6936 MVAr. The branch impedances and bus demands are taken from the classical data set reported by Savier and Das [26], which is commonly used for evaluating the performance of distribution power-flow methods in larger networks [6, 18, 27].

Table 3 reports the convergence results and power losses for the IEEE 69-bus feeder. As with the 33-bus case, the fixed-point iteration converged for all tested initial values. The number of iterations ranges from 15 (at $|q^{(0)}| = 0.1$ p.u.) to 12–13 for the remaining cases. The final voltage magnitudes and power losses are identical across all cases.

The total active power loss is 225.0718 kW, and the total reactive power loss is 102.3559 kVAr. The minimum voltage magnitude is 0.909194 p.u. at bus 65, which is within the acceptable range. The overall maximum voltage magnitude is 1.000000 p.u. at the slack bus. Among the non-slack buses, the maximum voltage magnitude is 0.999966 p.u. at bus 2.

Table 2. IEEE 33-bus feeder: per-branch power losses for the reference case ($|q^{(0)}| = 1.0$ p.u.).

Branch	From	To	P_{loss} (kW)	Q_{loss} (kVAr)	$\|I\|$ (p.u.)
1	1	2	12.3003	6.3636	4.624095
2	2	3	52.0768	26.5243	4.114645
3	3	4	20.0534	10.2130	2.963381
4	4	5	18.8501	9.6007	2.815603
5	5	6	38.5656	33.2917	2.747209
6	6	7	1.9462	6.4332	1.290840
7	7	8	11.8733	8.5688	1.054491
8	8	9	4.2657	3.0646	0.814719
9	9	10	3.6197	2.5755	0.746883
10	10	11	0.5650	0.1868	0.678700
11	11	12	0.8992	0.2973	0.620431
12	12	13	2.7210	2.1409	0.545053
13	13	14	0.7442	0.9795	0.469279
14	14	15	0.3643	0.3243	0.314336
15	15	16	0.2873	0.2098	0.248390
16	16	17	0.2568	0.3429	0.178707
17	17	18	0.0542	0.0425	0.108974
18	2	19	0.1610	0.1536	0.396616
19	19	20	0.8322	0.7499	0.297781
20	20	21	0.1008	0.1177	0.198589
21	21	22	0.0436	0.0577	0.099326
22	3	23	3.1820	2.1742	1.063161
23	23	24	5.1443	4.0621	0.958203
24	24	25	1.2876	1.0075	0.479922
25	6	26	2.6020	1.3254	1.433308
26	26	27	3.3304	1.6957	1.370473
27	27	28	11.3057	9.9680	1.308079
28	28	29	7.8367	6.8271	1.249736
29	29	30	3.8973	1.9851	1.109429
30	30	31	1.5943	1.5757	0.512098
31	31	32	0.2133	0.2486	0.331807
32	32	33	0.0132	0.0205	0.078690

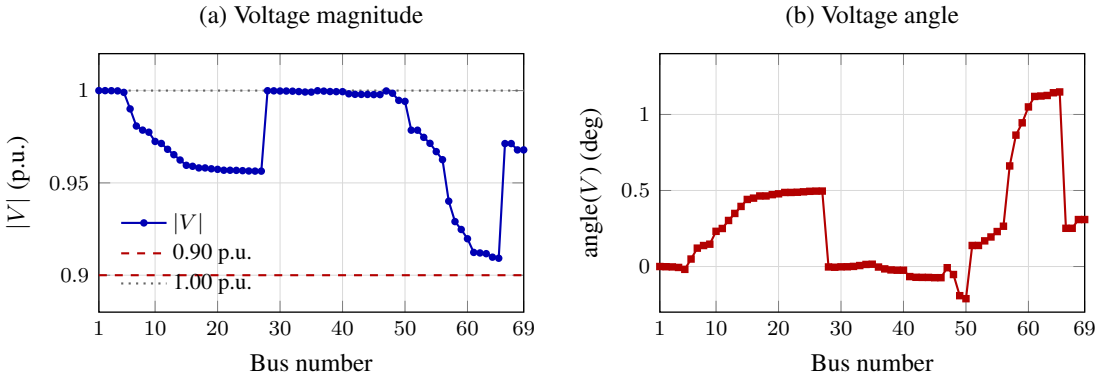

Figure 3. IEEE 69-bus voltage profile for the reference case ($|q^{(0)}| = 1.0$ p.u.).

Fig. 3 shows the voltage profile for the reference case ($|q^{(0)}| = 1.0$ p.u.). The voltage magnitudes decrease from the slack bus to the end of the feeder, with a minimum of 0.909194 p.u. at bus 65. The voltage angles are negative and increase in magnitude toward the end of the feeder.

Table 3. IEEE 69-bus feeder: convergence results and power losses as a function of the initial voltage magnitude.

Case	$\lvert q^{(0)}\rvert$ (p.u.)	Conv.	$\min \lvert V\rvert$ (p.u.)	$\max \lvert V\rvert$ (p.u.)	P_{loss} (kW)	Q_{loss} (kVAr)	Iter.
1	0.1	Yes	0.909194	1.000000	225.0718	102.3559	15
2	0.2	Yes	0.909194	1.000000	225.0718	102.3559	14
3	0.3	Yes	0.909194	1.000000	225.0718	102.3559	13
4	0.4	Yes	0.909194	1.000000	225.0718	102.3559	13
5	0.5	Yes	0.909194	1.000000	225.0718	102.3559	13
6	0.6	Yes	0.909194	1.000000	225.0718	102.3559	13
7	0.7	Yes	0.909194	1.000000	225.0718	102.3559	13
8	0.8	Yes	0.909194	1.000000	225.0718	102.3559	12
9	0.9	Yes	0.909194	1.000000	225.0718	102.3559	12
10	1.0	Yes	0.909194	1.000000	225.0718	102.3559	12
11	1.1	Yes	0.909194	1.000000	225.0718	102.3559	12
12	1.2	Yes	0.909194	1.000000	225.0718	102.3559	12
13	1.3	Yes	0.909194	1.000000	225.0718	102.3559	12
14	1.4	Yes	0.909194	1.000000	225.0718	102.3559	13
15	1.5	Yes	0.909194	1.000000	225.0718	102.3559	13
16	1.6	Yes	0.909194	1.000000	225.0718	102.3559	13
17	1.7	Yes	0.909194	1.000000	225.0718	102.3559	13
18	1.8	Yes	0.909194	1.000000	225.0718	102.3559	13
19	1.9	Yes	0.909194	1.000000	225.0718	102.3559	13

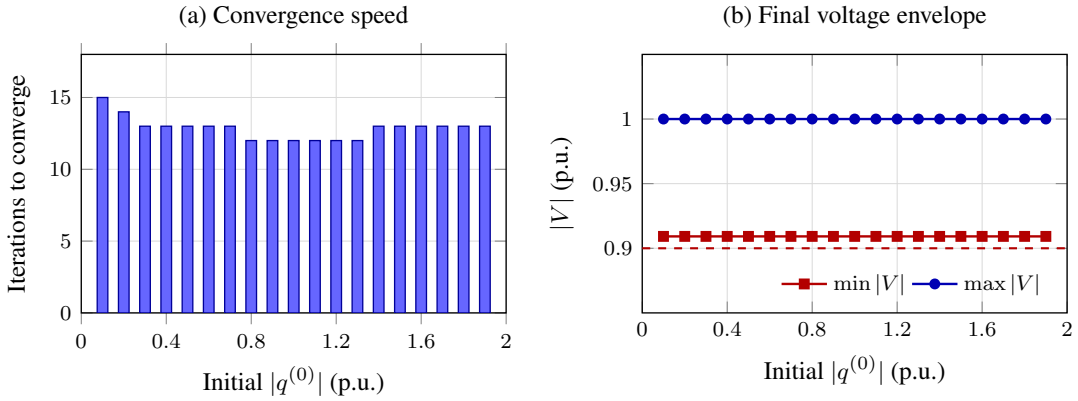

Figure 4. IEEE 69-bus feeder: (a) iterations to converge and (b) final voltage envelope, as functions of the initial voltage magnitude.

Fig. 4 shows the convergence behavior as a function of the initial voltage magnitude. As in the 33-bus case, the number of iterations decreases as the initial guess approaches the nominal value, and the final voltage envelope and power losses are invariant across all cases.

Table 4 reports the per-branch power losses for the reference case. The largest losses occur on branches 56 (49.68 kW), 6 (29.33 kW), 5 (28.22 kW), and 57 (24.49 kW), which correspond to the sections of the feeder that carry the largest currents.

5.3. Comparison with Classical Methods

To further assess the correctness of the proposed voltage-ratio fixed-point formulation, Table 5 compares the total active power losses and the minimum voltage magnitudes obtained for both test feeders with the results reported in the classical literature. The comparison is one of computed solutions, not of computational performance; no

Table 4. IEEE 69-bus feeder: per-branch power losses for the reference case ($|q^{(0)}| = 1.0$ p.u.).

Branches 1–34				**Branches 35–68**			
Br.	P_{loss} (kW)	Q_{loss} (kVAr)	$\lvert I\rvert$ (p.u.)	Br.	P_{loss} (kW)	Q_{loss} (kVAr)	$\lvert I\rvert$ (p.u.)
1	0.0772	0.1854	4.975627	35	0.0027	0.0067	0.314595
2	0.0772	0.1854	4.975627	36	0.0321	0.0784	0.283332
3	0.1949	0.4677	4.563092	37	0.0418	0.0488	0.252234
4	1.9355	2.2671	3.515583	38	0.0121	0.0141	0.252234
5	28.2233	14.3739	3.515583	39	0.0006	0.0007	0.223775
6	29.3305	14.9385	3.512160	40	0.1739	0.2031	0.195604
7	6.8903	3.5124	3.460886	41	0.0201	0.0235	0.102044
8	3.3729	1.7172	3.311381	42	0.0027	0.0031	0.102044
9	4.7655	1.5751	0.965710	43	0.0005	0.0006	0.094650
10	1.0122	0.3347	0.930914	44	0.0061	0.0077	0.094650
11	2.1847	0.7220	0.701565	45	0.0000	0.0000	0.047325
12	1.2801	0.4225	0.446305	46	0.0233	0.0575	1.047693
13	1.2413	0.4102	0.436534	47	0.5828	1.4266	1.047693
14	1.2021	0.3972	0.426734	48	1.6335	3.9970	0.950485
15	0.2234	0.0739	0.426734	49	0.1159	0.2835	0.475373
16	0.3204	0.1059	0.370338	50	0.0018	0.0009	0.055087
17	0.0026	0.0009	0.297973	51	0.0000	0.0000	0.004599
18	0.1041	0.0344	0.225693	52	5.7812	2.9438	2.307636
19	0.0669	0.0219	0.225693	53	6.7114	3.4185	2.301923
20	0.1074	0.0355	0.224478	54	9.1246	4.6458	2.268446
21	0.0005	0.0002	0.078327	55	8.7900	4.4778	2.237915
22	0.0051	0.0017	0.071948	56	49.6840	16.6770	2.237915
23	0.0112	0.0037	0.071948	57	24.4889	8.2182	2.237915
24	0.0060	0.0020	0.035979	58	9.5056	3.1435	2.237915
25	0.0025	0.0008	0.035979	59	10.6709	3.2391	2.104670
26	0.0003	0.0001	0.017990	60	14.0261	7.1443	2.104670
27	0.0003	0.0007	0.103239	61	0.1121	0.0571	0.429401
28	0.0020	0.0050	0.071360	62	0.1349	0.0687	0.386193
29	0.0039	0.0013	0.039626	63	0.6612	0.3368	0.386193
30	0.0007	0.0002	0.039626	64	0.0412	0.0210	0.079656
31	0.0034	0.0011	0.039626	65	0.0026	0.0008	0.045719
32	0.0082	0.0028	0.039626	66	0.0000	0.0000	0.022860
33	0.0069	0.0023	0.025476	67	0.0233	0.0077	0.071103
34	0.0003	0.0001	0.005662	68	0.0000	0.0000	0.035552

Table 5. Comparison of total active power losses and minimum voltage magnitudes with classical results.

Feeder	Method	P_{loss} (kW)	$\min \lvert V\rvert$ (p.u.)	Bus
IEEE 33-bus	Baran & Wu [25]	202.67	0.903778	18
	Proposed	210.99	0.903778	18
IEEE 69-bus	Savier & Das [26]	224.95	0.909194	65
	Proposed	225.07	0.909194	65

runtime, iteration-count, or memory comparison against NR, BFS, HELM, or current-injection methods has been performed in this work.

For the IEEE 69-bus feeder, the total active power loss is 225.07 kW, which is very close to the classical value of 224.95 kW reported in [26]. For the IEEE 33-bus feeder, the computed loss is 210.99 kW, which differs slightly from the classical value of 202.67 kW reported in [25]. This difference is consistent with the demand aggregation convention described in Section 5.1 (the demand is assigned to the receiving bus of each branch, which may differ slightly from the standard formulation), and the per-branch losses in Table 2 allow the reader to verify the total. The

minimum voltage magnitudes agree exactly with the classical results in both cases, in agreement with the values reported in [14, 15].

5.4. Discussion

The numerical results support the theoretical properties of the proposed voltage-ratio fixed-point formulation:

1. **Empirical convergence to a single solution.** For both test feeders, all initial voltage magnitudes (from 0.1 to 1.9 p.u.) converge to the same physical solution, with machine-precision agreement (error below 10^{-12} p.u.). The theorem establishes uniqueness only inside the certified ball $\mathcal{D}_\rho$; the observation that all tested initial points converge to the same solution is an empirical finding consistent with, but not implied by, the theorem. This is also consistent with the theoretical results reported in [16, 19] for fixed-point and sweep-based power-flow methods.
2. **Convergence speed.** The number of iterations remains low for all tested initial values: between 11 and 14 for the 33-bus feeder, and between 12 and 15 for the 69-bus feeder. The minimum iteration count occurs at $|q^{(0)}| = 0.9$ p.u. for the 33-bus feeder and at $|q^{(0)}| = 1.0$–1.3 p.u. for the 69-bus feeder. This is consistent with the contraction property: the iteration converges fastest when the initial guess is close to the solution. No runtime comparison with BFS, NR, HELM, or current-injection methods is reported in this work; the observed iteration counts are comparable to those reported in [4, 6] for BFS, but this is an observation, not a benchmark.
3. **Power losses.** The total active power losses are 210.99 kW (33-bus) and 225.07 kW (69-bus). The reactive power losses are 143.13 kVAr and 102.36 kVAr, respectively. The 33-bus value differs from the classical result of [25] by the demand aggregation convention described in Section 5.1; the 69-bus value is very close to the classical result of [26].
4. **Voltage profile.** The minimum voltage magnitudes are 0.903778 p.u. (33-bus, bus 18) and 0.909194 p.u. (69-bus, bus 65), both within the acceptable range of 0.90–1.10 p.u. The voltage angles are negative and increase in magnitude toward the end of the feeder, as expected for radial distribution networks.
5. **Robustness within the tested range.** The method converges for all tested initial values, including very low (0.1 p.u.) and above-nominal (1.9 p.u.) magnitudes. This observation is limited to the tested range, at nominal loading, with flat initial angles. It does not establish robustness near voltage collapse, under heavy loading, or for angle initialization far from zero; those cases are not examined in this work (see Section 5.5).
6. **Computational structure.** The iteration count is modest (11–15) for all cases, and each iteration requires only one linear solve. The matrix $\mathbf{Y}_{LL}$ is constant across iterations, so its factorization can be computed once and reused. This is a structural property of the iteration; it does not, by itself, establish a runtime advantage over any particular method, and no runtime measurements are reported in this work.

It is worth emphasizing that the convergence observed for all tested initial values does not contradict the fact that the certified conditions of Theorem 1 are sufficient rather than necessary. The certified region $\mathcal{D}_\rho$ provides a provable guarantee of convergence; the empirical results show that the actual basin of attraction is larger than the certified region, which is the expected behavior for a sufficient condition of this kind. A quantitative comparison between the certified radius and the empirical basin of attraction is not included in this work and is identified as future work in Section 5.5.

The numerical results also illustrate the practical relevance of the proposed formulation for modern distribution systems with distributed energy resources. Unlike classical BFS methods [4, 16], the derivation of the proposed formulation does not require a radial topology and can accommodate meshed configurations with a unique slack bus at the theoretical level. Unlike Newton–Raphson methods [3], it does not require the computation of the Jacobian matrix, which simplifies the implementation. The certified contraction radius derived in Section 3 provides a theoretical guarantee of convergence that is absent in most empirical approaches [14, 19]. These features make the proposed method a relevant candidate for real-time applications in active distribution networks with high penetration of renewable generation [1, 2], although a full assessment of its practical performance against established solvers remains to be carried out.

5.5. Scope and Limitations of the Present Validation

For transparency, this subsection summarizes the scope and the limitations of the validation reported above. The purpose is to allow the reader, the reviewers, and the editor to judge the actual evidence supporting each claim of the paper.

- **Radial-only validation.** Both test feeders are radial. No meshed or weakly meshed test system is analyzed. The topology-agnostic character of the formulation and of the convergence analysis is therefore a theoretical property, not an empirically validated one.
- **System size.** The largest test system has 69 buses. No large-scale test (e.g., 118-bus or 300-bus systems) is included, and scalability to large systems is not demonstrated.
- **Certificate not evaluated on the test systems.** The certified radius and the contraction factor are not numerically evaluated for the test feeders. The reported iteration counts demonstrate the empirical behavior of the iteration, not the certified one. The procedure for computing the certificate is described in Section 4, so that it can be reproduced by any reader; its numerical evaluation on the test systems is deferred to future work.
- **No same-platform benchmarking.** No runtime, iteration-count, or memory comparison against NR, BFS, HELM, or current-injection methods has been performed on the same platform. The comparison in Table 5 is a comparison of computed solutions, not of computational performance.
- **No stressed or near-collapse conditions.** All tests are at nominal loading. No loading sweep toward collapse is performed, and the behavior of the reciprocal operation as voltages approach zero is discussed theoretically (Remark 1) but not tested. No claim of robustness near voltage collapse is made.
- **Limited initial-condition sweep.** The sweep is restricted to the initial voltage magnitude, with a flat initial angle. Angle initialization, load stress, and ill-conditioned cases are not examined.
- **No PV buses, multiple slacks, or islanded operation.** The formulation assumes a unique slack bus and PQ injections at all non-slack buses. Voltage-controlled buses, distributed energy resources with voltage control, multiple slack buses, and islanded microgrids are outside the scope of the present formulation.
- **No real-world feeder.** No real utility feeder is tested. The validation is restricted to standard IEEE benchmark systems.
- **Dense implementation.** The simulations were performed with a dense MATLAB implementation. A sparse implementation is expected to be beneficial for large systems, but it has not been benchmarked in this work.
- **Conservatism of the certificate.** The sources of conservatism of the certificate are discussed in Section 3.0.7, but no quantitative parametric study of the gap between the certified radius and the empirical basin of attraction is included.

The above limitations delimit the scope of the claims made in this paper. They are also the natural starting point for the future work outlined in Section 6.

5.6. Summary of Numerical Findings

The proposed voltage-ratio fixed-point power-flow method has been validated on two standard radial distribution test feeders: the IEEE 33-bus and IEEE 69-bus radial networks. For both feeders, the method converges to the same power-flow solution for all tested initial voltage magnitudes, with the number of iterations remaining between 11 and 15. The computed voltage profiles agree with the classical benchmark results, and the computed active power losses are consistent with them once the demand aggregation convention described in Section 5.1 is taken into account. These results support the correctness of the formulation for radial networks. The theoretical analysis is topology-agnostic, but meshed-network validation is not included in this work and is identified as future work.

6. Conclusions

This paper proposed a voltage-ratio fixed-point formulation for the power-flow analysis of balanced AC distribution networks with either radial or meshed topologies at the theoretical level. The classical nodal power-flow equations

were recast exactly in terms of inverse squared-voltage magnitude variables and pairwise complex voltage-ratio variables, and then compactly normalized with respect to the unique slack-bus voltage. The resulting normalized power-flow equations define a fixed-point mapping whose nonlinearity is confined to an element-wise reciprocal of the conjugated normalized voltage vector.

A rigorous convergence analysis was developed using the Banach fixed-point theorem. Sufficient conditions for the existence, uniqueness, and at-least-linear convergence of the fixed-point iteration were derived explicitly in terms of the reduced nodal admittance matrix, the normalized complex power injections, the no-load voltage profile, and a certified contraction radius. The derivation does not rely on radiality assumptions, parent–child relationships, or backward/forward sweep orderings, and therefore applies, at the theoretical level, to radial and meshed networks with a unique slack bus, provided that the reduced nodal admittance matrix is nonsingular. The derived contraction factor also provides a priori and a posteriori error bounds with a direct theoretical interpretation, including a computable a priori bound expressed in terms of the certified radius and the contraction factor.

The proposed formulation was validated on the IEEE 33-bus and IEEE 69-bus radial distribution test feeders. The method converged to the same power-flow solution for all tested initial voltage magnitudes (from 0.1 to 1.9 p.u.), with machine-precision agreement and iteration counts between 11 and 15. The computed voltage profiles agree with the classical benchmark results, and the computed active power losses are consistent with them once the demand aggregation convention described in the text is taken into account. These results support the correctness of the formulation for radial networks.

The scope of the present validation is limited, and this is stated explicitly in Section 5.5: the tests are radial, of moderate size (33 and 69 buses), at nominal loading, with a flat initial angle, and without a numerical evaluation of the certificate on the test systems or a same-platform benchmarking against NR, BFS, HELM, or current-injection methods. The corresponding claims of the paper have been narrowed accordingly.

Future work will address the limitations identified above and extend the proposed formulation in several directions: (i) numerical validation on meshed and weakly meshed test systems, to substantiate the topology-agnostic character of the analysis; (ii) large-scale tests, including the 118-bus system and larger cases, with a sparse implementation and a formal runtime and memory comparison against established sparse solvers; (iii) numerical evaluation of the certificate on the test systems, together with a parametric study of the gap between the certified radius and the empirical basin of attraction; (iv) analysis and testing under heavy loading and near voltage collapse, including safeguards for the reciprocal operation; (v) validation on real-world distribution system data; (vi) extension to three-phase unbalanced distribution networks, to networks with multiple slack buses or islanded microgrids [28], and to the analysis of convergence in the presence of voltage-controlled (PV) buses; and (vii) integration of the proposed method with optimization and control algorithms for active distribution networks.

ACKNOWLEDGEMENTS

The authors acknowledge the support provided by Thematic Network 723RT0150 “Red para la integración a gran escala de energías renovables en sistemas eléctricos (RIBIERSE-CYTED)” funded by the 2022 Call for Thematic Networks by the Ibero-American Program of Science and Technology for Development (CYTED in Spanish).

Declaration of AI Use

The authors acknowledge the assistance of the DeepSeek AI language model in refining the manuscript’s language and structure. The tool was used solely for editorial purposes—such as rephrasing, grammar correction, and improving readability—whereas all technical formulations, methodological developments, numerical simulations, and scientific interpretations were conceived and executed by the authors.

REFERENCES

[1] Pavel Ilyushin, Sergey Filippov, and Konstantin Suslov. Features of planning and managing power flows in distribution grids of megalopolises. *Renewable Energy*, 235:121330, Nov 2024. ISSN 0960-1481. 10.1016/j.renene.2024.121330.

[2] Ayesha, Gabriele Mosaico, and Federico Silvestro. Power Flow Methods for Efficient Analysis of Modern Distribution Networks—Review. *Energies*, 19(16):3902, Aug 2026. ISSN 1996-1073. 10.3390/en19163902.

[3] Nien-Che Yang and Chih-Hsiung Tseng. Adaptive convergence enhancement strategies for newton–raphson power flow solutions in distribution networks. *IET Generation, Transmission & Distribution*, 18(13):2339–2352, June 2024. ISSN 1751-8695. 10.1049/gtd2.13197.

[4] E. Bompard, E. Carpaneto, G. Chicco, and R. Napoli. Convergence of the backward/forward sweep method for the load-flow analysis of radial distribution systems. *International Journal of Electrical Power & Energy Systems*, 22(7):521–530, Oct 2000. ISSN 0142-0615. 10.1016/s0142-0615(00)00009-0.

[5] D. Shirmohammadi, H.W. Hong, A. Semlyen, and G.X. Luo. A compensation-based power flow method for weakly meshed distribution and transmission networks. *IEEE Transactions on Power Systems*, 3(2):753–762, May 1988. ISSN 0885-8950. 10.1109/59.192932.

[6] A. Augugliaro, L. Dusonchet, S. Favuzza, M.G. Ippolito, and E. Riva Sanseverino. A backward sweep method for power flow solution in distribution networks. *International Journal of Electrical Power & Energy Systems*, 32(4):271–280, May 2010. ISSN 0142-0615. 10.1016/j.ijepes.2009.09.007.

[7] S. Elsaiah, M. Ben-Idris, and J. Mitra. Power flow analysis of radial and weakly meshed distribution networks. In *2012 IEEE Power and Energy Society General Meeting*, pages 1–9. IEEE, July 2012. 10.1109/pesgm.2012.6345739.

[8] Tao Shen, Yanjun Li, and Ji Xiang. A graph-based power flow method for balanced distribution systems. *Energies*, 11(3):511, Feb 2018. ISSN 1996-1073. 10.3390/en11030511.

[9] Oscar Danilo Montoya, Walter Gil-González, and Alexander Molina-Cabrera. Relation between the branch-to-node incidence and triangular matrices in radial distribution networks. *Ingeniería*, 28(1):e20108, Jan 2023. ISSN 0121-750X. 10.14483/23448393.20108.

[10] Oscar Danilo Montoya-Giraldo, Walter Gil-González, and Edwin Rivas-Trujillo. Evaluation on the equivalence between the backward/forward iterative sweep and the triangular-based power flow methods in electrical distribution networks. *Revista UIS Ingenierías*, 23(4), 2024. ISSN 2145-8456. 10.18273/revuin.v23n4-2024009.

[11] P.M. De Oliveira-De Jesus, M.A. Alvarez, and J.M. Yusta. Distribution power flow method based on a real quasi-symmetric matrix. *Electric Power Systems Research*, 95:148–159, Feb 2013. ISSN 0378-7796. 10.1016/j.epsr.2012.08.011.

[12] Diego Issicaba and Jorge Coelho. Rotational Load Flow Method for Radial Distribution Systems. *International Journal of Electrical and Computer Engineering (IJECE)*, 6(3):1344, June 2016. ISSN 2088-8708. 10.11591/ijece.v6i3.pp1344-1352.

[13] Attia A. El-Fergany. Reviews on Load Flow Methods in Electric Distribution Networks. *Archives of Computational Methods in Engineering*, 32(3):1619–1633, Oct 2024. ISSN 1886-1784. 10.1007/s11831-024-10191-7.

[14] L.F. Grisales-Noreña, J.C. Morales-Duran, S. Velez-Garcia, Oscar Danilo Montoya, and Walter Gil-González. Power flow methods used in ac distribution networks: An analysis of convergence and processing times in radial and meshed grid configurations. *Results in Engineering*, 17:100915, Mar 2023. ISSN 2590-1230. 10.1016/j.rineng.2023.100915.

[15] Oscar Danilo Montoya, Alexander Molina-Cabrera, and Jesus C. Hernández. A comparative study on power flow methods applied to ac distribution networks with single-phase representation. *Electronics*, 10(21):2573, Oct 2021. ISSN 2079-9292. 10.3390/electronics10212573.

[16] Bohang Fang, Changhong Zhao, and Steven H. Low. Convergence of backward/forward sweep for power flow solution in radial networks. *IEEE Transactions on Control of Network Systems*, 12(2):1780–1792, June 2025. ISSN 2372-2533. 10.1109/tcns.2025.3534557.

[17] Yuntao Ju, Wenchuan Wu, and Boming Zhang. Convergence problem in forward/backward sweep power flow method caused by non-positive-sequence impedance of distributed generators and its solution. *International Journal of Electrical Power & Energy Systems*, 65:463–466, Feb 2015. ISSN 0142-0615. 10.1016/j.ijepes.2014.04.035.

[18] M. Shamseldein. A fast holomorphic embedding power flow approach for meshed distribution networks. *International Transactions on Electrical Energy Systems*, 2022:1–11, June 2022. ISSN 2050-7038. 10.1155/2022/9561385.

[19] Oscar Danilo Montoya and Walter Gil-González. On the numerical analysis based on successive approximations for power flow problems in AC distribution systems. *Electric Power Systems Research*, 187:106454, Oct 2020. ISSN 0378-7796. 10.1016/j.epsr.2020.106454.

[20] Daniel-Leon Schultis and Clemens Korner. A method for the modular power flow analysis of extensive distribution grids. *Energies*, 18(6):1559, Mar 2025. ISSN 1996-1073. 10.3390/en18061559.

[21] Kamna Singh, Khyati D. Mistry, Hirenkumar G. Patel, and Sabha Raj Arya. Advanced load flow techniques for mesh distribution systems: A detailed study of current injection and iterative nodal methods. In *Renewable Energy Integration with Electric Vehicle Technology*, pages 641–665. Springer Nature Singapore, 2026. ISBN 9789819587735. 10.1007/978-981-95-8773-5_33.

[22] Mohammed Amin Hakmi and Mohamed Nour. A Fractional SEIAQR Model under Caputo and Atangana–Baleanu Operators: Dynamics, Sensitivity, and Estimation for the 2024 Algeria Diphtheria Outbreak. *Statistics, Optimization & Information Computing*, 16(5), 2026. ISSN 2311-004X. 10.19139/soic-2310-5070-4585.

[23] Tharmalingam Gunasekar, Jaya Priya Dhanasekar, Nidal Anakira, Osama Ogilat, and Amani Sheimat. Variable-order fractional differential equations: Existence, stability, and application to 3d noise evolution. *Statistics, Optimization & Information Computing*, 16(1):641–659, 2026. ISSN 2311-004X. 10.19139/soic-2310-5070-4095.

[24] Cristian David Cuervo-Gonzalez, John Fredy Pinilla-Morales, and Oscar Danilo Montoya Giraldo. Power Flow Analysis in Unbalanced Distribution Networks with Single-Phase and Two-Phase Laterals Using a Fixed-Point Formulation Implemented in MATLAB. *Statistics, Optimization & Information Computing*, 16(3):2465–2490, 2026. ISSN 2311-004X. 10.19139/soic-2310-5070-3443.

[25] M. E. Baran and F. F. Wu. Network reconfiguration in distribution systems for loss reduction and load balancing. *IEEE Transactions on Power Delivery*, 4(2):1401–1407, 1989. 10.1109/61.25627.

[26] J. S. Savier and D. Das. Impact of network reconfiguration on loss allocation of radial distribution systems. *IEEE Transactions on Power Delivery*, 22(4):2473–2480, 2007. 10.1109/TPWRD.2007.905370.

[27] A. Al-Sakkaf and M. AlMuhaini. Power flow analysis of weakly meshed distribution network including dg. *Engineering, Technology & Applied Science Research*, 8(5):3398–3404, Oct 2018. ISSN 2241-4487. 10.48084/etasr.2277.

[28] Elson Natanael Moreira Silva, Anselmo Barbosa Rodrigues, and Maria da Guia da Silva. Multi-slack power flow for islanded microgrids with radial and meshed topologies. *IET Generation, Transmission & Distribution*, 14(13):2498–2509, May 2020. ISSN 1751-8695. 10.1049/iet-gtd.2019.1777.